Nearly Rigid Descriptor-Based Matching for Volume Reconstruction from Histological Sections

Shaohui Sun[a], Nzola De Magalhães[b], and Nathan D. Cahill[c]

[a]Center for Imaging Science
[b]Department of Biomedical Engineering
[c]Center for Applied and Computational Mathematics, School of Mathematical Sciences
Rochester Institute of Technology, Rochester, NY 14623, USA

ABSTRACT

A common task in the analysis of digitized histological sections is reconstructing a volumetric representation of the original specimen. Image registration algorithms are used in this task to compensate for translational, rotational, scale, shear, and local geometric differences between slices. Various systems have been developed to perform volumetric reconstruction by registering pairs of successive slices according to rigid,[1–3] similarity,[4] affine,[5,6] and/or deformable[7–10] transformations. To provide a coarse initial volumetric reconstruction, rigid transformations may be too constrained, as they do not allow for scale or shear; but, affine transformations may be too flexible, enabling larger scale or shear factors than physically reflected in the histological sections.

One difficulty with these systems is caused by the *aperture problem*; even if successive slices are registered reasonably well, the composition of transformations over tens or hundreds of slices can yield global twisting and scale and shear changes that yield a volumetric reconstruction that is significantly distorted from the shape of the true specimen. The impact of the aperture problem can be reduced by considering more than two successive images in the registration process. Systems that take this approach use global energy functions,[11] elastic spring models,[12] post hoc filtering/smoothing,[13,14] or solutions to shortest-path problems on graphs.[15]

In this article, we propose a volume reconstruction algorithm that handles the aperture problem and yields *nearly* rigid transformations (i.e., affine transformations with small scale and shear factors). Our algorithm is based on robust geometric alignment of descriptive feature points (for example, using SIFT[16]) via constrained optimization. We will illustrate our algorithm on the task of volumetric reconstruction from histological sections of a chicken embryo with an embedded tumor spheroid.

Keywords: Registration, histology, volume reconstruction

1. INTRODUCTION

In histology and histopathology, biological specimens are sectioned and stained so that they can be viewed to study the structure of tissues and cells. To complement the information observed in each section, it is useful to virtually reconstruct the three-dimensional specimen from digitized sections. This is not a straightforward task because subsequent histology slides are not perfectly aligned and because there may be stretching or tearing of tissue in different sections. Without the availability of a prior CT or MR image of the specimen to serve as a guide, the only way to form a virtual reconstruction is to use an image registration algorithm to align the digitized sections.

A variety of reconstruction approaches have been proposed that use image registration to perform pairwise alignment subsequent sections. The sections are assumed to be related by rigid,[1–3] similarity,[4] affine,[5,6] or deformable transformations,[7–9,13] and the image registration algorithm optimizes intensity[2,3,7,9] or feature[4] based similarity measures or a combination of both.[1,8] While these techniques may be able to register pairs of slices accurately, they all suffer from the *aperture problem*; namely, small local errors can propagate over many slices to yield a global reconstruction with significant distortion in rotation, scale, and shear. Malandain et al.[17] and Cifor et al.[10] provide good descriptions of the aperture problem and show how it can lead to the erroneous

Send correspondence to Nathan D. Cahill: nathan.cahill@rit.edu

Medical Imaging 2012: Image Processing, edited by David R. Haynor, Sébastien Ourselin,
Proc. of SPIE Vol. 8314, 831417 · © 2011 SPIE · CCC code: 0277-786X/11/$18 · doi: 10.1117/12.911665

reconstruction of a cylinder from digitized sections of a banana. Some strategies have been developed for tackling the aperture problem in the absence of a prior volumetric image with which to compare the reconstruction. These strategies include the use of global energy functions,[11] elastic spring models,[12] post hoc filtering/smoothing,[13,14] or shortest-path problems on graphs.[15]

In this article, we propose an algorithm for volume reconstruction from histological sections that combines two key features. First, it allows for *nearly* rigid transformations between sections; that is, transformations between sections are affine, but nonrigid components such as scale and shear can be penalized by an amount controlled by the user. Second, it reduces the impact of the aperture problem by enforcing consistency of transformations across three or more sections. The proposed algorithm has three general steps:

1. Extract descriptive features (e.g., using SIFT[16]) from every image.
2. Use a robust technique (e.g., RANSAC[18]) to identify affine feature correspondences between each pair of images at most M slices apart.
3. Solve an optimization problem to find a nearly rigid transformation that best aligns all feature correspondences while simultaneously ensuring that the transformations are consistent in every M-neighborhood of slices.

The remainder of this article is organized as follows. Section 2 briefly summarizes a number of the prior art systems for volume reconstruction from histological sections. Section 3 details the proposed algorithm, describing how to enable nearly rigid transformations that are consistent across multiple slices. Section 4 illustrates how the proposed algorithm is used to perform a volumetric reconstruction from histological sections of a chicken embryo with an embedded tumor spheroid. Finally, Section 5 provides conclusions and ideas for future work.

2. BACKGROUND

The problem of volumetric reconstruction from two-dimensional biological images has a rich history in the research literature. In this section, we provide a brief review of some key algorithms and systems for volumetric reconstruction, focusing on those algorithms that do not rely on comparison with another three-dimensional image of the specimen.

One of the earliest fully automatic volumetric reconstruction techniques was published in 1988 by Hibbard and Hawkins,[1] who propose using the centroids and principal axes of each image, or alternatively the cross-correlation between successive images, to rigidly register successive autoradiographs of the brain. Later reconstruction approaches based on rigid registration of successive images include Ourselin et al.,[2] who use block-matching with local correlation coefficients followed by robust estimation of rigid transformations from motion vectors to generate reconstructions of rat and rhesus monkey brains, and Mosaliganti et al.,[3] who successively register sections of mouse placenta by maximizing the mutual information between neighboring sections.en successive images, to rigidly register successive autoradiographs of the brain. Later reconstruction approaches based on rigid registration of successive images include Ourselin et al.,[2] who use block-matching with local correlation coefficients followed by robust estimation of rigid transformations from motion vectors to generate reconstructions of rat and rhesus monkey brains, and Mosaliganti et al.,[3] who successively register sections of mouse placenta by maximizing the mutual information between neighboring sections.

Other volumetric reconstruction algorithms have been based on computing similarity or affine transformations between slices. Both types of transformations are more flexible than rigid transformations; similarity transformations enable scale changes, and affine transformations enable both scale and shear changes. Rangarajan et al.[4] estimate similarity transformations between autoradiographs from points extracted from Canny edges. The point correspondences are estimated in a robust manner as part of the optimization process. Zhao et al.[5] use disparity analysis to align contours of 2-D coronal autoradiographic sections according to an affine model in order to measure cerebral blood flow. Goldszal et al.[6] minimize a least squares objective function to perform affine registration of sections of the cerebral cortex of a rat.

Still other algorithms use deformable transformations between slices. Pitiot et al.[7] propose a general purpose algorithm that uses robust block matching followed by hierarchical clustering in order to perform a hybrid local

affine/nonlinear registration between slices. Schmitt et al.[8] coarsely align sections of a mouse brain using the principal axes transformation, then refine these results with a rigid + shear transformation by minimizing the sum of squared differences between slices, and finally perform elastic registration. Bagci and Bai[9] standardize image intensities and subsequently use properties of edges in each slice in order to perform local affine registration (the affine transformation varies spatially within each slice) of mouse brain sections.

To mitigate the aperture problem, there seem to be two common strategies: smoothing local features[10,14] or local transformations[13] to make the global transformation more regular, and simultaneously considering three or more (or all!) of the slices in a neighborhood to generate a more globally consistent transformation.[11,12,15] The first strategy includes the methods of Ju et al.,[13] who generate smooth warps across the sequence of sections by Gaussian filtering the warps estimated from pairwise sections, Tan et al.,[14] who smooth feature curves across slices using nonuniform rational B-splines (NURBS), and Cifor et al,,[10] who evolve feature boundaries with mean curvature flow. The second strategy includes the early work of Guest and Baldock,[12] who treat each slice as a thin elastic plate and consider point correspondences between slices as connections between springs, ultimately solving a finite element method (FEM) model for the equilibrium of the spring system. In addition, this strategy includes the more recent work of Krinidis et al.,[11] who construct and minimize a global energy function from distance transforms of object contours to measure the similarity between all pairs of slices, and Yushkevich et al.,[15] who rigidly align each slice with five slices in each direction by maximizing the mutual information between slices, construct a graph whose edge weights are related to the MI values, and determine the optimal path to a reference slice.

3. METHODS

The proposed algorithm for volumetric reconstruction of histology sections will meet two goals: first, it will estimate *nearly rigid* transformations between images of successive sections, and second, it will reduce the impact of the aperture problem. The first goal will be addressed with the use affine transformations in a way that allows a user-controlled penalty for non-unit scale and nontrivial shear. The second goal will be addressed by constraining the estimation to be consistent across neighborhoods of images.

To meet these goals, we propose an algorithm comprised of the following three steps: (1) feature extraction, (2) feature matching, (3) optimization. The first two steps are not unique to this problem and can utilize any of a variety of robust feature extraction and matching strategies known in the art. The optimization step provides the key to meeting the two goals of our algorithm: the objective function is designed in a way that penalizes non-unit scale and nontrivial shear, and constraints are designed to enforce consistency across neighborhoods of images.

3.1 Feature Extraction

Let $\{I_j\}|_{j=1}^{N}$ be a series of images (histological sections) that are represented as functions from $\mathcal{R}^2$ to $\mathcal{R}$. Ultimately, in order to perform the optimization step, we need to identify locations of corresponding points (or of more general features) across images. Let $\left\{\left(\mathbf{u}_i^{(j,k)}, \mathbf{v}_i^{(j,k)}\right)\right\}\Big|_{i=1}^{N_{j,k}}$ be a set of ordered pairs in $\mathbb{R}^2 \times \mathbb{R}^2$ that denote corresponding points between images I_j and I_k, and assume that $\mathbf{u}_i^{(j,k)} \in \mathcal{F}_j$ and $\mathbf{v}_i^{(j,k)} \in \mathcal{F}_k$, where $\mathcal{F}_j$ and $\mathcal{F}_k$ are sets of feature locations extracted from images I_j and I_k, respectively.

To construct a list $\mathcal{F}$ of feature locations for each image, we use the scale-invariant feature transform (SIFT)[16] to generate keypoints. SIFT identifies keypoints as maxima of a difference of Gaussians function applied to the scale space representation of the image, and it generates feature vectors that are invariant to translation, scaling, and rotation of the image. SIFT is one of a number of feature descriptors that are used in various computer vision applications; other feature descriptors include the speeded up robust feature (SURF)[19] and the histogram of oriented gradients (HOG).[20]

Figure 1 shows images of three successive sections of a chicken embryo as well as locations of SIFT keypoints that have been extracted for each image. The SIFT keypoints were found using the publicly available code provided by David Lowe.[21] The number of keypoints extracted were 526 for the left image, 404 for the middle image, and 551 for the right image. Note that some of the SIFT keypoints appear to be located outside of the boundary of the chicken embryo. These keypoints represent features with large scale factors.

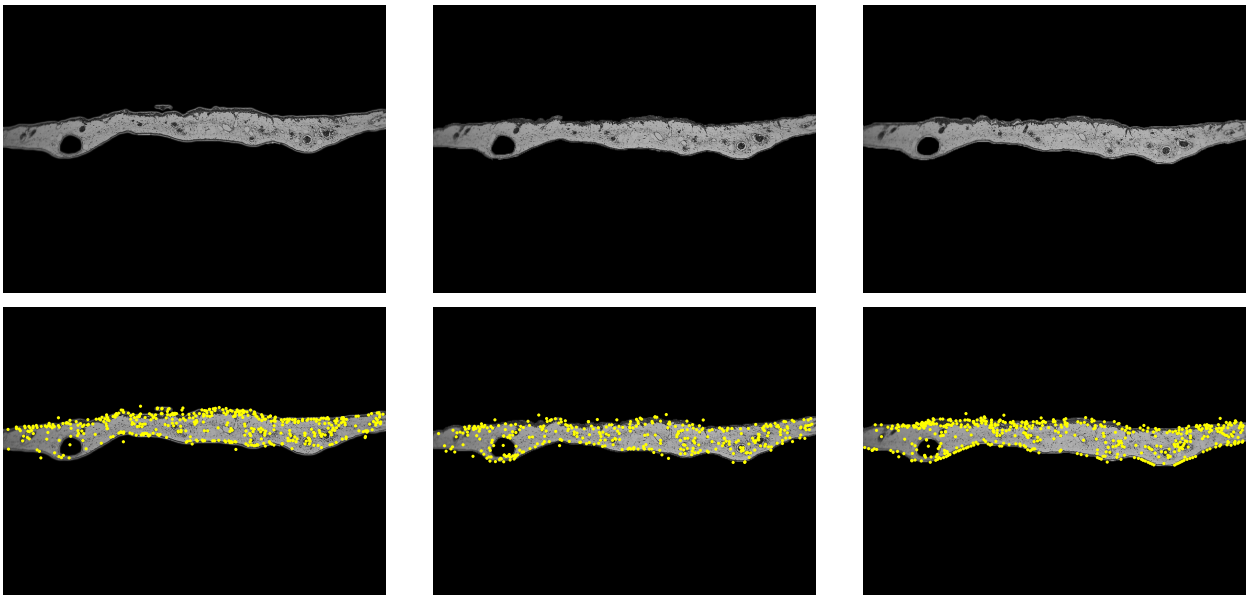

Figure 1. (Top) Three successive histological sections of the chorioallantoic membrane (CAM) of a chicken embryo; (bottom) locations of SIFT keypoints superimposed.

3.2 Feature Matching

Once a list $\mathcal{F}$ of feature locations is constructed for each image, we need to identify corresponding features in pairs of images. To do this in a robust manner, we first use the SIFT features at each keypoint in order to identify a list of putative matches. This is done by identifying all SIFT features in the second image whose normalized dot product with the SIFT feature at hand in the first image is above a threshold. Once the putative matches are are found for each SIFT feature, we use the random sample consensus (RANSAC) algorithm[18] to find the best set of feature matches that fits an affine transformation. The locations of these features generate the $\left\{\left(\mathbf{u}_i^{(j,k)}, \mathbf{v}_i^{(j,k)}\right)\right\}\Big|_{i=1}^{N_{j,k}}$ ordered pairs necessary for the subsequent optimization.

Figure 2 shows the resulting locations of corresponding features between each pair of the chicken embryo images. In yellow "x"'s are the 17 corresponding features between the left and middle images, in green "o"'s are the 25 corresponding features between the middle and right images, and in red "+"'s are the 10 corresponding features between the left and right images. Note that the three sets of pairwise correspondences do not overlap; in general, there may be some corresponding features between images I_i and I_k that do not exist in the lists of corresponding features between either I_i and I_j or I_j and I_k.

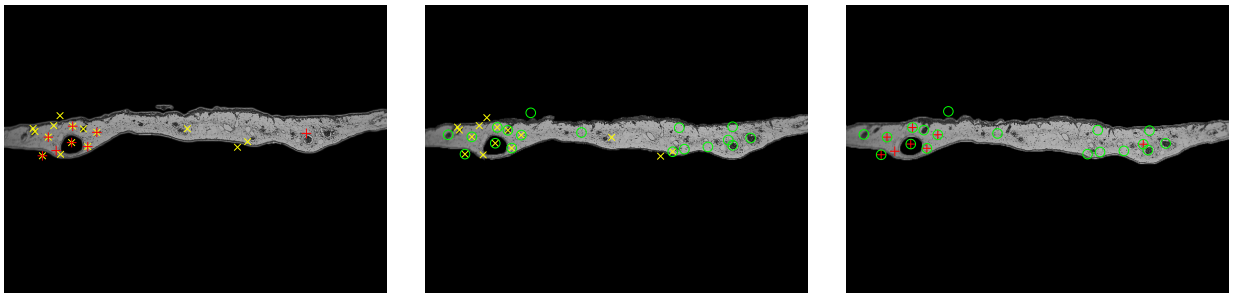

Figure 2. Histological sections with locations of corresponding SIFT keypoints superimposed. Yellow "x"'s indicate correspondences between the middle and right images, green "o"'s the middle and right images, and red "+"'s the middle and right images.

3.3 Optimization

Once we have performed the first two steps of our algorithm for generate corresponding points between every pair of images that are no more than M slices apart, we are ready to estimate affine transformations between each pair of slices. If we consider I_j and I_k to be related by an affine transformation, then $\mathbf{v}_i^{(j,k)} = \mathbf{A}_{j,k}\mathbf{u}_i^{(j,k)} + \mathbf{t}_{j,k}$, for $i = 1, 2, \ldots, N_{j,k}$, where $\mathbf{A}_{j,k}$ is a 2×2 matrix that applies rotation, scaling, and shear, and $\mathbf{t}_{j,k}$ is a 2×1 translation vector. For simplicity, we will denote $\mathcal{A}_{j,k}$ as the affine transform described by $\mathbf{A}_{j,k}$ and $\mathbf{t}_{j,k}$.

3.3.1 Energy Function for Nearly Rigid Transformations

Now, to estimate the sequence of affine transforms $\{\mathcal{A}_{j,j+1}\}_{j=1}^{N-1}$, we first design an energy term that penalizes errors between true and predicted corresponding point locations:

$$\mathcal{E}_{\text{features}}(\mathcal{A}) = \sum_{j=1}^{N-1} \sum_{k=j+1}^{\min(j+M,N)} \left[\frac{\alpha_{k-j}}{N_{j,k}} \sum_{i=1}^{N_{j,k}} \left(\mathbf{v}_i^{(j,k)} - \mathbf{A}_{j,k}\mathbf{u}_i^{(j,k)} - \mathbf{t}_{j,k} \right)^2 \right] , \tag{1}$$

where α_ℓ is the weight assigned to correspondence errors in images that are ℓ slices apart, and where $\mathcal{A} = \{\mathcal{A}_{j,k} | \, 1 \le j < k \le \min(j + M, N)\}$.

To enable the "nearly rigid" behavior and favor affine transformations with small amounts of non-unit scale and/or non-trivial shear, we define two new energy terms; namely,

$$\mathcal{E}_{\text{scale}}(\mathcal{A}) = \sum_{j=1}^{N-1} \beta_j \left(|\log \lambda_1(\mathbf{A}_{j,j+1})| + |\log \lambda_2(\mathbf{A}_{j,j+1})| \right) , \tag{2}$$

$$\mathcal{E}_{\text{shear}}(\mathcal{A}) = \sum_{j=1}^{N-1} \gamma_j \frac{\left| \mathbf{v}_{j,j+1}^{(1)} \cdot \mathbf{v}_{j,j+1}^{(2)} \right|}{\left\| \mathbf{v}_{j,j+1}^{(1)} \right\| \left\| \mathbf{v}_{j,j+1}^{(2)} \right\|} , \tag{3}$$

where $\lambda_1(\mathbf{A})$ and $\lambda_2(\mathbf{A})$ are the eigenvalues of $\mathbf{A}$, $\mathbf{v}^{(1)}$ and $\mathbf{v}^{(2)}$ are the corresponding eigenvectors, and β_j and γ_j are weights that define the relative influence of the transformation between images $\mathcal{I}_j$ and $\mathcal{I}_{j+1}$.

The scale term $\mathcal{E}_{\text{scale}}$ is identically zero for rigid transformations and grows as the eigenvalues of the transformation depart from unit magnitude. In the shear term $\mathcal{E}_{\text{shear}}$, the terms being multiplied by the γ_j's are the cosines of the angles between the eigenvectors of the transformations. Hence, $\mathcal{E}_{\text{shear}}$ is identically zero when the eigenvectors of the transformations are orthogonal. (In theory, affine transformations could be defective, as is the case with pure shear. However, in these cases, the two eigenvectors can be chosen from the same one-dimensional eigenspace, so the cosine of the angle between them will be maximal.)

The energy terms can be linearly combined to form the energy function to be minimized:

$$\mathcal{E}_{\alpha,\beta,\gamma}(\mathcal{A}) = \alpha\mathcal{E}_{\text{features}}(\mathcal{A}) + \beta\mathcal{E}_{\text{scale}}(\mathcal{A}) + \gamma\mathcal{E}_{\text{shear}}(\mathcal{A}) , \tag{4}$$

where α, β, and γ are global weights that define the relative contribution of the energy terms (1)–(3).

3.3.2 Consistency Constraints

If we attempt to minimize (4) directly, we will identify an inconsistent solution. For example, we know that it must be true that $\mathcal{A}_{1,3} = \mathcal{A}_{2,3} \circ \mathcal{A}_{1,2}$, but there is no guarantee that this constraint will be preserved. Therefore, the appropriate strategy is to perform a constrained minimization; namely:

$$\begin{aligned} \min_{\mathcal{A}} \quad & \mathcal{E}_{\alpha,\beta,\gamma}(\mathcal{A}) \\ \text{subject to} \quad & \mathcal{A}_{j,k+1} = \mathcal{A}_{k,k+1} \circ \mathcal{A}_{j,k}, \quad 1 \le j < k \le \min(j + M, N) \end{aligned} . \tag{5}$$

Equation (5) is a nonlinear minimization problem with quadratic constraints. Its solution can be found via Sequential Quadratic Programming (SQP), or by any of a variety of other constrained optimization techniques.[22]

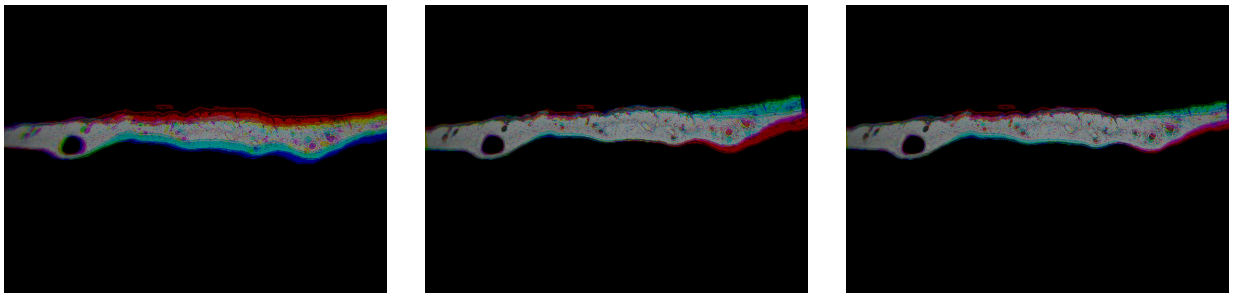

Figure 3. Blended versions of the three histological sections from Fig. 1 under no registration (left), registration without consistency constraint (middle), and registration with consistency constraint (right). The three histological sections are color coded red, green, and blue.

Any such technique requires an initial estimate of the solution; in this case, the affine transformations found in the robust feature correspondence step provide a suitable initialization.

Figure 3 shows the resulting registration of the three histological sections of the chicken embryo from the top of Fig. 1. On the left, we see the results of blending the three sections together with no registration. In the middle, registration has been performed *without* the consistency constraint. On the right, registration has been performed *with* the consistency constraint. In each case, the sections have been color coded red, green, and blue so that the blended images should have color fringes in areas of misregistration.

4. RECONSTRUCTION EXAMPLE

To illustrate the behavior of the proposed algorithm on more than three images, we apply it to the problem of volume reconstruction of a biological tissue sample containing a human tumor spheroid embedded in the chorioallantoic membrane of a chicken embryo. The tissue sample was formalin fixed, paraffin embedded and serial sectioned into slices of 6μm thickness each. The sections were histologically stained (hematoxylin and eosin) and two-dimensional images of each section were captured via an Olympus bright-field microscope equipped with a 1.3 megapixel color digital camera. The first three sections in the sequence were illustrated in Fig.'s 1–3. Other example sections from the sequence are shown in Fig. 4.

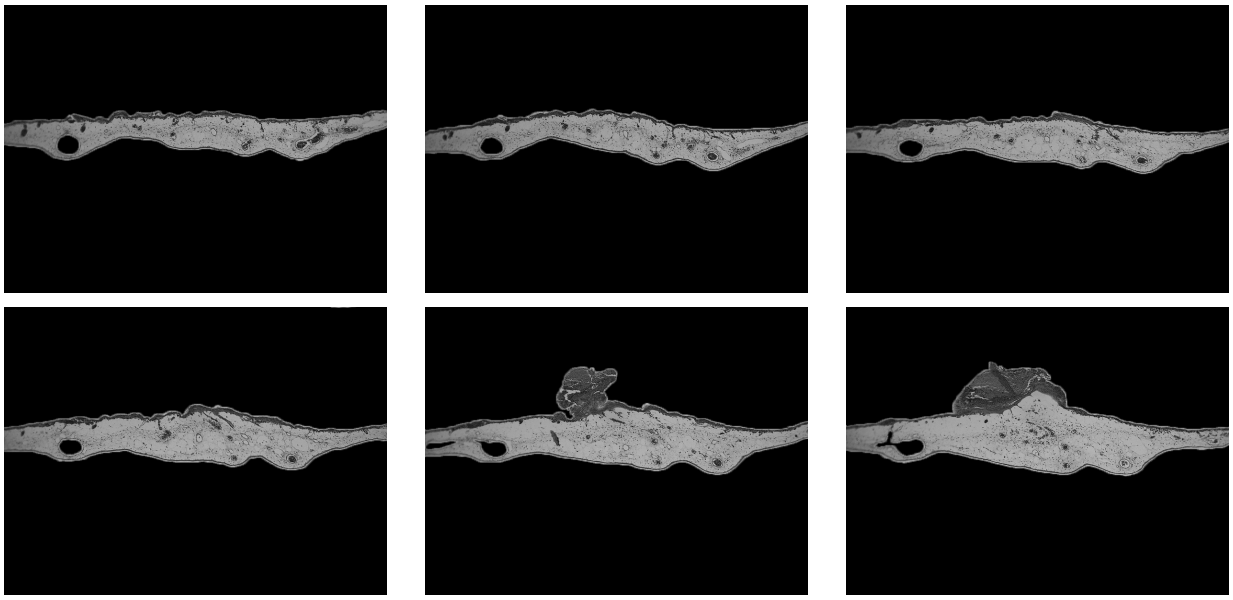

Figure 4. Slices 8, 16, 24, 32, 40, and 48 of the dataset of histological sections of the chorioallantoic membrane (CAM) of a chicken embryo.

We applied various parameterizations of the proposed algorithm to generate volume reconstructions from images of 50 successive histological sections. The digital images of each section were 600×800 pixels. On average, we extracted 500 SIFT features from each image, and RANSAC generated approximately 20 corresponding points between each pair of images. To solve the constrained optimization problem, we used the SQP algorithm implemented in the `fmincon` function in MATLAB's Optimization Toolbox.[23]

As can be seen in Fig. 5(a), a registration step is necessary in order to generate a physically realistic reconstruction. To provide a baseline comparison to a straightforward pairwise registration algorithm, we performed only the first two steps of our proposed algorithm (SIFT + RANSAC with $M = 1$). The resulting reconstruction is shown in Fig. 5(b). Note that even though some of the sections have been successfully registered, a single erroneous affine transformation can be catastrophic.

Figure 5(c) shows the results of the proposed algorithm (for $M = 2$) when the constrained optimization is applied solely to the $\varepsilon_{\text{features}}$ energy term; i.e., $\beta = \gamma = 0$ in (5). With the change from pairwise registration to globally consistent triplet-wise registration, we see that single erroneous affine transformations are no longer catastrophic. However, the flexibility inherent in affine transformations is apparent in the side view; notice the slight decrease in scale and downward shear when moving rightward through the slices.

Finally, Fig. 5(d) shows the volume reconstruction generated by the proposed algorithm (for $M = 2$) when all energy terms are treated equally in the constrained optimization; i.e., $\alpha = \beta = \gamma = 1$. We now see that in addition to achieving a globally consistent result, we have also achieved a result with less distortion than in Fig. 5(c).

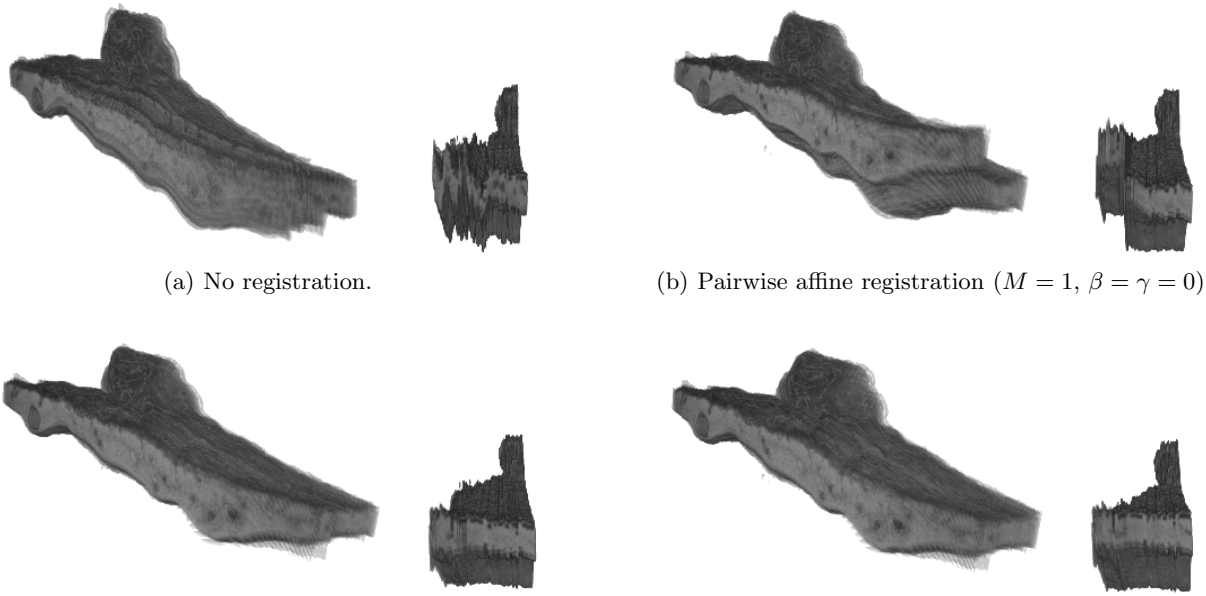

(a) No registration.

(b) Pairwise affine registration ($M = 1$, $\beta = \gamma = 0$).

(c) Proposed algorithm with $M = 2$, $\alpha = 1$, $\beta = \gamma = 0$.

(d) Proposed algorithm with $M = 2$, $\alpha = \beta = \gamma = 1$.

Figure 5. Volume reconstructions of a portion of a chicken embryo from 50 histological sections of 6μm thickness. Reconstruction are shown from diagonal and side views.

To quantify the *nearly rigid* nature of our algorithm, we note that the singular values of any two dimensional rigid transformation must both be equal to one. Hence, the extent to which the singular values differ from one can be used as a proxy for measuring how much the transformation differs from being rigid. We are free to choose any image in the sequence as the reference image. Figure 6 illustrates the singular values of $\mathcal{A}_{j,k}$ for all images k when j is chosen to be the first image, the middle image, and the last image in the sequence, respectively. For comparison, it also illustrates the singular values of the affine transformations computed without the energy terms for scale and shear (i.e., when $\beta = \gamma = 0$ in (5)). As can be seen in the figure, when slice 1 is chosen as the

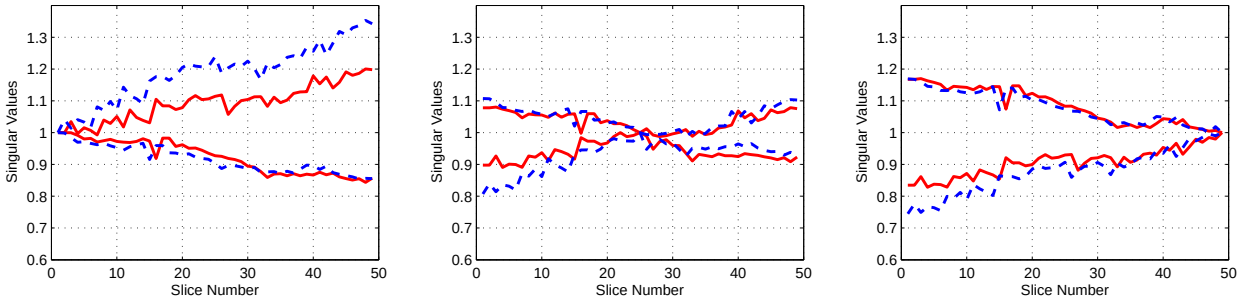

Figure 6. Plots of the two singular values of the cumulative affine transformation found by nearly rigid registration (red solid lines) and by affine registration with no energy terms to penalize scale or shear (blue dashed lines). The chosen reference slice, where both singular values are one by definition, is slice 1 (left), slice 25 (middle), and slice 50 (right).

reference, the larger singular value is clearly drawn closer to unity by our proposed algorithm, and when slice 50 is chosen as the reference, the smaller singular value is clearly drawn closer to unity.

5. CONCLUSIONS AND FUTURE WORK

Volume reconstruction from histological sections is a challenging problem that has attracted many researchers. Standard techniques for reconstruction align successive sections according to some geometric transformation model, such as rigid, similarity, affine, or deformable models. One problem with such techniques is that rigid and similarity transformations are not necessarily general enough to encompass the range of expected deformations, however affine transformations tend to be too flexible in allowing large scale and shear components. Furthermore, these techniques can fall victim to the aperture problem, where acceptable errors in local registration results can propagate to unacceptable global errors in the reconstruction.

In this paper, we proposed an algorithm for addressing these two issues. First, it registers successive sections according to a *nearly rigid* transformation, by using an affine transformation that is biased towards having small scale and shear components. Second, it reduces the impact of the aperture problem by constraining the resulting transformations to be consistent across neighborhoods containing multiple sections. The algorithm involves feature extraction, feature matching, and optimization steps, the first two of which can utilize well known prior art techniques. The optimization step involves minimizing a nonlinear energy function subject to quadratic constraints, a process that can be performed by sequential quadratic programming. We illustrated the algorithm on a sequence of histological sections of the chorioallantoic membrane of a chicken embryo.

One potential area of future work involves the inclusion of intensity-based similarity measures into the energy function. (These could be included in place of or in addition to the feature-based term.) The constrained optimization framework would be equally valid, and the optimization problem could still be solved via sequential quadratic programming. Another potential area of future work would be the use of this algorithm as a coarse alignment step that is followed by a deformable registration technique or some feature-smoothing algorithm.

REFERENCES

[1] Hibbard, L. S. and Hawkins, R. A., "Objective image alignment for three-dimensional reconstruction of digital autoradiograms," *Journal of Neuroscience Methods* **26**, 55–74 (November 1988).

[2] Ourselin, S., Roche, A., Subsol, G., Pennec, X., and Ayache, N., "Reconstructing a 3D structure from serial histological sections," *Image and Vision Computing* **19**, 25–31 (2000).

[3] Mosaliganti, K., Pan, T., Sharp, R., Ridgway, R., Iyengar, S., Gulacy, A., Wenzel, P., de Bruin, A., Machiraju, R., Huang, K., Leone, G., and Saltz, J., "Registration and 3D visualization of large microscopy images," in [*Proc. SPIE Medical Imaging: Image Processing*], **6144**, 61442V–1–61442V–12 (2006).

[4] Rangarajan, A., Chui, H., Mjolsness, E., Pappu, S., Davachi, L., Goldman-Rakic, P., and Duncan, J., "A robust point-matching algorithm for autoradiograph alignment," *Medical Image Analysis* **1**(4), 379–398 (1997).

[5] Zhao, W., Young, T. Y., and Ginsberg, M. D., "Registration and three-dimensional reconstruction of autoradiographic images by the disparity analysis method," *IEEE Transactions on Medical Imaging* **12**, 782–791 (December 1993).
[6] Goldszal, A. F., Tretiak, O. J., Hand, P. J., Bhasin, S., and McEachron, D. L., "Three-dimensional reconstruction of activated columns from 2-[^{14}C] deoxy-D-glucose data," *NeuroImage* **2**, 9–20 (March 1995).
[7] Pitiot, A., Bardinet, E., Thompson, P., and Malandain, G., "Piecewise affine registration of biological images for volume reconstruction," *Medical Imaging Analysis* **10**, 465–483 (2006).
[8] Schmitt, O., Modersitzki, J., Heldmann, S., Wirtz, S., and Fischer, B., "Image registration of sectioned brains," *International Journal of Computer Vision* **73**(1), 5–39 (2007).
[9] Bagci, U. and Bai, L., "Registration of standardized histological images in feature space," in [*Proc. SPIE Medical Imaging: Image Processing*], **6914**, 69142V–1–69142V–9 (2008).
[10] Cifor, A., Pridmore, T., and Pitiot, A., "Smooth 3-D reconstruction for 2-D histological images," in [*Proc. Information Processing in Medical Imaging*], *LNCS* **5636**, 350–361 (2009).
[11] Krinidis, S., Nikou, C., and Pitas, I., "A global energy function for the alignment of serially acquired slices," *IEEE Transactions on Information Technology in Biomedicine* **7**(2), 108–113 (2003).
[12] Guest, E. and Baldock, R., "Automatic reconstruction of serial sections using the finite element method," *Bioimaging* **3**, 154–167 (1995).
[13] Ju, T., Warren, J., Carson, J., Bello, M., Kakadiaris, I., Chiu, W., Thaller, C., and Eichele, G., "3D volume reconstruction of a mouse brain from histological sections using warp filtering," *Journal of Neuroscience Methods* **156**, 84–100 (2006).
[14] Tan, Y., Hua, J., and Dong, M., "Feature curve-guided volume reconstruction from 2D images," in [*Proc. International Symposium on Biomedical Imaging*], 716–719 (2007).
[15] Yushkevich, P. A., Avants, B. B., Ng, L., Hawrylycz, M., Burstein, P. D., Zhang, H., and Gee, J. C., "3D mouse brain reconstruction from histology using a coarse-to-fine approach," in [*Proc. Workshop on Biomedical Image Registration*], **4057**, 230–237 (2006).
[16] Lowe, D. G., "Distinctive image features from scale-invariant keypoints," *International Journal of Computer Vision* **60**(2), 91–110 (2004).
[17] Malandain, G., Bardinet, E., Nelissen, K., and Vanduffel, W., "Fusion of autoradiographs with an MR volume using 2-D and 3-D linear transformations," *NeuroImage* **23**, 111–127 (2004).
[18] Fischler, M. A. and Bolles, R. C., "Random sample consensus: A paradigm for model fitting with applications to image analysis and automated cartography," *Communications of the ACM* **24**, 381–395 (1981).
[19] Bay, H., Ess, A., Tuytelaars, T., and Van Gool, L., "SURF: Speeded up robust features," *Computer Vision and Image Understanding* **110**(3), 346–359 (2008).
[20] Dalal, N. and Triggs, B., "Histograms of oriented gradients for human detection," in [*Proc. Computer Vision and Pattern Recognition*], **1**, 886–893 (June 2005).
[21] `http://www.cs.ubc.ca/~lowe/keypoints`.
[22] Fletcher, R., [*Practical Methods of Optimization*], Wiley, 2$^{\text{nd}}$ ed. (May 2000).
[23] `http://www.mathworks.com`.